

**A Wind Profiler Assisted Case Study
of a Nonprecipitating Warm Front**

by
Steven M. London
Thomas B. McKee

Department of Atmospheric Science
Colorado State University
Fort Collins, Colorado



**Department of
Atmospheric Science**

Paper No. 526

**A WIND PROFILER ASSISTED CASE STUDY OF A
NONPRECIPITATING WARM FRONT**

Steven M. London

Thomas B. McKee

Atmospheric Science Department
Colorado State University
Fort Collins, CO 80523

April 1993

Atmospheric Science Paper #526

A WIND PROFILER ASSISTED CASE STUDY OF A NONPRECIPITATING WARM FRONT

ABSTRACT

Wind profiler data collected during FIRE-II, in November, 1991, provided an opportunity for detailed observation of the passage of a warm front over Parsons, KS. Surface data, rawinsonde data and satellite observations were used to collaborate and understand the phenomena detected by the wind profiler. A quality-controlled set of wind profiler data were produced from the time-averaged spectra and the spectral moments derived from the time-averaged spectra. Using the wind profiler data set, the warm frontal zone was clearly identifiable as a low level, descending layer of veering winds over Parsons, KS. The warm frontal zone exhibited a relatively smooth surface, without the apparent height discontinuities observed by other researchers. Above the layer of warm advection, there was an abrupt transition to a layer of cold advection. The temperature gradient across this transition zone resulted in a layer of decreased stability. A study of the origin of the warm and cold advective zones found that the warm advection originated west-southwest of Parsons, in a region of warmer, but dry air, while the cold advection was from geostrophic flow around a strong cyclone far to the northeast of Parsons. The interaction between the northwesterly geostrophic flow and the southwesterly advective flow resulted in horizontal deformation, leading to frontogenesis.

ACKNOWLEDGEMENTS

The authors would like to thank Professor Stephen Cox and Professor Jon Peterka for their advice and suggestions. They would also like to thank Paul Hein, Research Associate, CSU Department of Atmospheric Science, who provided invaluable assistance in obtaining the wind profiler, surface and rawinsonde data from the FIRE-II field experiment supported by NASA Grant NAG-1-1146. Paul provided some of the software used in this study and spent a great deal of time patiently answering many questions about wind profilers. Professor Roger Pielke provided suggestions for studying warm fronts. Steve Finley, CSU Department of Atmospheric Science, helped use GEMPAK to analyze rawinsonde data and produce many of the figures in this paper.

Steve London would like to acknowledge that his graduate tuition was paid by AT&T Bell Laboratories, under the Special Enhanced Leave of Absence program. And special thanks goes to his wife, Kathy, who provided the continual support and encouragement to begin and persevere through this Master's program, despite the drastic change in our lifestyle.

TABLE OF CONTENTS

	<u>Page</u>
1 INTRODUCTION	1
1.1 General Background	1
1.1.1 Wind Profilers	2
1.1.1.1 Quality Control of Wind Profiler Data	4
1.1.1.2 Calculation of Kinematic Quantities	7
1.1.2 Warm Fronts	8
1.1.2.1 Classical Theories	8
1.1.2.2 Warm Front Models Based on Primitive Equations	9
1.1.2.3 Previous Observational Studies	10
2 SYNOPTIC METEOROLOGICAL ANALYSIS	11
2.1 Upper Air	11
2.2 Surface	12
2.3 Satellite Observations	14
3 WIND PROFILER OBSERVATIONS, PROCESSING AND ANALYSIS ...	32
3.1 Wind Profiler Data Processing	32
3.2 Warm Front Placement Using Wind Profiler Data	35
3.2.1 Verification	36
3.3 Warm Front Thermal Advection	36
3.4 Interactions Between Warm and Cold Advection Zones	39
3.5 Vertical Velocity Profile	40
3.6 Isentropic Trajectory Analysis	41
3.7 Frontogenesis	44
4 DISCUSSION AND CONCLUSIONS	73
4.1 Three-Dimensional Structure of the Parsons, KS Warm Front	73
4.2 Comparison With Other Warm Front Observational Studies	73
4.2.1 Comparison with Chicago Warm Front (Heymsfield, 1979)	74
4.2.2 Comparison with Washington Warm Front (Hobbs and Locatelli, 1987)	75
4.3 Conclusions	75
4.4 Suggestions for Future Research	77
REFERENCES	79
APPENDIX A	83

LIST OF FIGURES

<u>Number</u>	<u>Caption</u>	<u>Page</u>
Figure 2.1	- 1200 UTC 23 November 500 mb Analysis	15
Figure 2.2	- 0000 UTC 25 November 500 mb Analysis	16
Figure 2.3	- 0000 UTC 25 November 310 Degree Isentropic Analysis	17
Figure 2.4	- 1200 UTC 25 November 310 Degree Isentropic Analysis	18
Figure 2.5	- 1800 UTC 25 November 310 Degree Isentropic Analysis	19
Figure 2.6	- 1200 UTC 26 November 500 mb Analysis	20
Figure 2.7	- 0000 UTC 25 November 700 mb Analysis	21
Figure 2.8	- 0000 UTC 26 November 700 mb Analysis	22
Figure 2.9	- 2100 UTC 24 November Surface Analysis	23
Figure 2.10	- 2100 UTC 25 November Surface Analysis	24
Figure 2.11	- 1800 UTC 26 November Surface Analysis	25
Figure 2.12	- 25 November Parsons KS Surface Temperature	26
Figure 2.13	- 25 November Parsons KS Wind Direction	27
Figure 2.14	- 25 November Parsons KS Downward Infrared Radiation	28
Figure 2.15	- 0300 UTC 25 November Satellite Infrared Image	29
Figure 2.16	- 0900 UTC 25 November Satellite Infrared Image	30
Figure 2.17	- 2100 UTC 25 November Satellite Infrared Image	31
Figure 3.1	- Parsons, KS Wind 0000 UTC - 0700 UTC 25 November	47
Figure 3.2	- Parsons, KS Wind 0800 UTC - 1500 UTC 25 November	48
Figure 3.3	- Parsons, KS Wind 1600 UTC - 2300 UTC 25 November	49
Figure 3.4	- Neodesha, KS Wind Profiler 25 November	50
Figure 3.5	- 25 November Monett, MO Wind	51
Figure 3.6	- Parsons, KS Temperature Advection	52
Figure 3.7	- 0000 UTC to 2400 UTC Temperature Change	53
Figure 3.8	- 0000 UTC to 1200 UTC Temperature Change	54
Figure 3.9	- 1200 UTC to 1800 UTC Temperature Change	55
Figure 3.10	- 1800 UTC to 2400 UTC Temperature Change	56
Figure 3.11	- Monett, MO Sounding 1200 UTC	57
Figure 3.12	- Parsons, KS Sounding 1512 UTC	58
Figure 3.13	- Monett, MO Sounding 1800 UTC	59
Figure 3.14	- Parsons, KS Sounding 2008 UTC	60
Figure 3.15	- Relative Humidity Cross Section 1200 UTC	61
Figure 3.16	- Relative Humidity Cross Section 1800 UTC	62
Figure 3.17	- Parsons, KS Vertical Velocity	63
Figure 3.18	- 1800 UTC 25 November 285 K Isentropic Analysis.	64
Figure 3.19	- 1800 UTC 25 November 300 K Isentropic Analysis.	65
Figure 3.20	- 1200 UTC 25 November 285 K Isentropic Analysis.	66
Figure 3.21	- 1200 UTC 25 November 300 K Isentropic Analysis.	67
Figure 3.22	- Idealized Warm Frontogenesis	68
Figure 3.23	- 1200 UTC 25 November 850 mb Frontogenesis	69
Figure 3.24	- 1800 UTC 25 November 850 mb Frontogenesis	70
Figure 3.25	- 1200 UTC 25 November 700 mb Frontogenesis	71
Figure 3.26	- 1800 UTC 25 November 700 mb Frontogenesis	72

1 INTRODUCTION

The overrunning of warm air over cold air prior to the passage of a surface warm front can result in large amounts of precipitation. Orographic enhancement of the precipitation can cause significant flooding, despite the innocuous appearance of the warm front on the synoptic scale (Hobbs, Locatelli 1987). Considering the potential economic impact of warm front-associated weather, there has been a surprising lack of observational studies of warm fronts. Compared to cold fronts, warm fronts are generally not as well defined and can be difficult to locate. In the past, this has led some meteorologists to doubt their existence.

The First ISCCP Regional Experiment - II (FIRE-II) provided an opportunity for the detailed observation of the passage of a warm front. From November 13, 1991 until December 7, 1992, the CSU wind profiler was in continuous operation and surface meteorological parameters were collected at Parsons, Kansas. In addition, rawinsondes were occasionally launched from Parsons during special study periods. Supplementing the standard NWS soundings at 0000 UTC and 1200 UTC, NWS rawinsondes were launched daily at 1800 UTC.

This thesis uses the data from FIRE-II to examine a warm front that passed through Parsons, Kansas on November 25, 1991. The CSU wind profiler was used as the primary instrument to study the front. Surface data and rawinsonde data were used to collaborate and understand the phenomena detected by the wind profiler. Section 2 provides a synoptic meteorological overview, incorporating upper air, surface and satellite observations. The processing and analysis of the wind profiler data, and study of the 25 November warm front are provided in Section 3. A comparison with other observational studies of warm fronts, and conclusions are presented in Section 4.

1.1 General Background

This section is subdivided into two sections. Section 1.1.1 describes the fundamental aspects of wind profiler operation. Commonly used procedures used to filter wind profiler data are presented. The computation of kinematic quantities from wind profiler data are described. Section 1.1.2 is a brief literature survey of warm fronts. Classical theories, numerical models, and previous observational studies are presented.

1.1.1 Wind Profilers

This section presents a brief overview of the principles and operation of wind profilers. For greater detail, the reader should consult other references (Van de Kamp 1988, Tycho 1988).

A wind profiler is a Doppler radar used to measure atmospheric winds above a site. Wind profilers depend upon the scattering of very high frequency (VHF) or ultra high frequency (UHF) electromagnetic radiation by minor irregularities in the index of refraction of air. These irregularities in the index of refraction are typically caused by turbulent eddies in the atmosphere. Since these turbulent eddies are carried by the wind, they are good "tracers" of the mean wind. The wind profiler transmits short pulses of electromagnetic radiation in a selected direction at a selected frequency. Echos are produced by the scattering of electromagnetic radiation. These echos are received from all heights within the range of operation of the profiler. The echos are sampled at selected times corresponding to distance and height from the profiler. The height associated with each sample is typically referred to as a "range gate" and corresponds to a volume of atmosphere illuminated by the electromagnetic radiation. By measuring the Doppler shift of the returned echo, the radial velocity of the turbulent eddies within the range gate can be deduced. Since there are turbulent eddies moving at various speeds

within the range gate (due to shear and turbulence), the echo is "spread out" in frequency. Several hundred samples are obtained and averaged to form a frequency spectra. The mean radial velocity is determined from the spectra by searching for a "spike" that contains the largest amount of power.

The radial velocity from a single wind profiler beam is clearly not sufficient to define the horizontal wind vector. In a typical wind profiler, three beams are used: one tilted to the east, one tilted to the north, and one vertical. The CSU wind profiler has two additional beams: one tilted to the south and one tilted to the west. The angle of the tilt is 75° from the horizon. For a three beam profiler, the wind vector is then calculated from

$$u = V_{east} \sec 75^\circ - w \tan 75^\circ \quad (1)$$

$$v = V_{north} \sec 75^\circ - w \tan 75^\circ \quad (2)$$

where V_{east} and V_{north} are the radial velocities determined from the east and north wind profiler beams. For the five-beam CSU wind profiler, equations (1) and (2) are also used, with appropriate modifications for the west and south beams.

A number of factors can affect the accuracy of wind profiler data and limit their applicability. These factors include:

- Radial wind velocities in excess of the Nyquist velocity (related to the pulse repetition frequency and number of samples used to derived the frequency spectra). For the CSU wind profiler, the Nyquist velocity is 28.9 m/s for when used in the low height mode, and 32.2 m/s when used in the high height mode.

- Nonuniform winds across the wind profiler beams, including nonuniformity caused by convection, lee waves and gravity waves. For example, the opposing beams of the CSU wind profiler, "illuminate" a volume of air separated by approximately 5400 m at a height of 10 km. During certain meteorological conditions, there can be a significant difference in wind velocity across a distance of 5400 m.
- An insufficient number of small scale eddies. As altitude increases, the density of the air decreases. As the density decreases, the Reynolds number of the atmosphere decreases. This decrease in Reynolds number with altitude places a lower limit on the size of the smallest eddies. This effectively limits the maximum height range of wind profilers.
- Low signal-to-noise ratio of received echo.
- Internally and externally generated electrical noise.
- Side lobes in the wind profiler antenna pattern.
- Hydrometeors, particularly liquid water.

A descriptive summary of wind profiler errors and limitations can be found in Van de Kamp (1988). Strauch, et al. (1987) discussed the effect of lee waves and gravity waves on horizontal wind accuracy. Wuertz, et al. (1988) discussed the effect of precipitation and Weber, et al. (1992) discussed the effect of nonuniform winds.

1.1.1.1 Quality Control of Wind Profiler Data

As discussed in the previous section, many factors can cause contamination of wind profiler data. Numerous methods have been devised to attempt to remove unrepresentative data from wind profiler data sets. Two methods have been used to provide quality control (QC) of wind profiler data from the NOAA demonstration

network. A third method has frequently been used to filter data obtained from the CSU wind profiler. In addition, the use of the CSU wind profiler to study this specific, synoptic scale event allows the use of unique quality control techniques which may not be generally applicable to other meteorological events or other wind profiler sites. These three methods, as well as others, were examined to determine their applicability to the 25 November, 1991 warm front case.

The first QC method was developed by Brewster and Schlatter (see Brewster (1989) and Brewster and Schlatter (1986, 1988)). The Brewster/Schlatter method uses the techniques of consensus averaging, median filter and shear checking. In the consensus averaging technique, an hourly average of the wind at a particular height level is derived from multiple 6-minute radial velocity samples. Each of the ten 6-minute radial velocity samples is examined to determine how many other radial velocity samples fall within a designated radial velocity "window" of the chosen 6-minute sample. The sample with the greatest number of other samples within the window is chosen. All of the samples within the window are then averaged to obtain the "consensus averaged" 1-hour average. If a consensus cannot be obtained (i.e. there are too few samples within the largest group of samples), the data for that hour, at that height, are flagged as bad.

The median filter and shear check are applied to consensus-averaged hourly data. In the median filter technique, data are gathered from adjacent hours and adjacent height levels. The median of this collection of data is computed for the two horizontal wind components. If the difference between the data and the median is greater than a threshold, then the median is recalculated using only data from the current hour and the previous hour. The data is flagged as bad if the observed data and the recalculated data differ by more than a threshold.

In the shear check technique, the vertical consistency between adjacent and nearby height levels is checked against a threshold. Three or four consecutive height levels are compared to determine if any of the wind vectors have an unacceptably large amount of shear between them.

The second QC method was developed by Wuertz and Weber (1989). The Wuertz/Weber method uses the techniques of continuity and pattern editing. The continuity technique is based on the expectation that wind measurements change smoothly from one height to another, and from one time to another. The "smoothness" is defined in terms of a maximum rotation between neighboring wind vectors. Greater rotation between neighboring wind vectors is permitted at lower wind velocities. The continuity technique also restricts the speed shear between neighboring wind vectors that have the same wind direction.

The pattern editing technique joins together those wind vectors in the neighborhood (i.e. nearby in time and space) that are continuous (as determined by the continuity technique) to form a pattern. A weight is assigned to each pattern, equal to the size of the pattern. By an iterative process, the pattern with the smallest weight is removed, removing that wind profiler data from the data set. Wind vector patterns and weights are recalculated. This process continues until all points are continuous.

The third QC method was developed at CSU by Hein (see Hein, et al. (1991)). The Hein method checks several characteristics of the radial velocity. If the variance of the radial velocity is less than a threshold, the data is marked as bad. If the echo signal power between the vertical, north and east beams deviates by more than a threshold, the data is marked as bad. A shear check is performed between adjacent height levels and time intervals for each radial velocity. If the percentage of spatial and temporal neighbors

that vary significantly from the subject radial velocity is greater than a threshold, the subject radial velocity is marked as bad.

The CSU wind profiler is a five beam profiler, rather than the more typical three beam profiler. By comparing the four wind velocities derived from the five beams, the uniformity of the derived wind field over the profiler can be tested. In nonconvective, nonprecipitating, synoptic scale events, far from a mountain barrier, the wind field should be uniform over the volume scanned by the wind profiler. Nonhomogeneous winds observed under these conditions are suggestive of bad data, and should be exploited as another quality control procedure. Quality control based on nonhomogeneous winds has not been used as a method of quality control in previous studies.

1.1.1.2 Calculation of Kinematic Quantities

Much of the earlier work using wind profilers studied the echo reflectivity strength in relation to atmospheric phenomena (Shapiro, et al. (1984), Rottger (1979), Larsen and Rottger (1983). More recent work has exploited the increased temporal resolution of the wind data provided by profilers to study the atmosphere.

The use of earlier technology, such as rawinsondes, provides high resolution wind data as a function of height. However, rawinsondes are typically launched only twice per day, and the geographic density of rawinsonde launch sites is fairly sparse. A single wind profiler provides the same high resolution data, but in a nearly continuous manner. From a single profiler, many kinematic quantities can be calculated. Neiman and Shapiro (1989) used a single wind profiler and the geostrophic form of the thermal wind equation to calculate the temperature gradient vector and temperature advection for an upper tropospheric front and jet stream passage. When the wind within the layer of interest is

not in geostrophic balance, the magnitude of the terms in the general form of the thermal wind equation must be considered (Forsythe, 1945).

A network of wind profilers expands the possibilities for calculation of kinematic quantities. Zamora, et al. (1987) used a network of three wind profilers to calculate upper tropospheric divergence and ageostrophic wind. The work by Zamora, et al. assumes that the wind field varies linearly throughout the region defined by the profiler network. They derived a method called the linear vector point function (LVPF) that allows the kinematic quantities of wind, divergence, vorticity and deformation at any point within a triangular wind profiler network to be calculated based on the three wind profiler observations, and the distance from the three wind profilers. Kuo, et al. (1987) simulated a network of wind profilers, each separated by 360 km, to calculate the temperature and geopotential fields using the divergence equation. They found that for synoptic situations with weak dynamic forcing, the retrieved fields are about as accurate as from the current rawinsonde network. For situations with strong dynamic forcing, the RMS errors can be approximately 50 % greater than the current rawinsonde network.

1.1.2 Warm Fronts

This section describes the classical theories of warm fronts, frontogenesis, numerical modelling of warm fronts based on the primitive equations, and previous observational studies.

1.1.2.1 Classical Theories

The origin of the classical theories of frontal development can be traced to work done by Bjerknes (1918) and Bjerknes and Solberg (1922). Bjerknes and Solberg were the first to present a detailed discussion of wave cyclones and their associated cold, warm and occluded fronts. Using a spatially dense network of surface data, Bjerknes (1918)

found zones of confluence associated with cold and warm fronts, and temperature gradients across these fronts. The well known patterns of clouds and precipitation associated with fronts was related to the adiabatic cooling of warm air lifted by the fronts. Bjerknes and Solberg (1922) were also the first to note the differences in vertical structure between cold and warm fronts. In particular, cold fronts are steeper and warm fronts can be difficult to locate at the surface.

Harrold (1973) introduced the concept of a "conveyor belt" of warm air, 100 to 1000 km wide, and several km in depth. The conveyor belt, is parallel to, and ahead of the surface cold front. As the air moves poleward, it rises up over the warm front. Most of the warm frontal precipitation is caused by condensation within the ascending portion of the conveyor belt.

There have been many papers discussing the banded nature of precipitation embedded within warm fronts (Herzogh and Hobbs (1980), Houze, et al. (1981), Rutledge and Hobbs (1983), Heymsfield (1979)). However, in general, there has been very little attention paid to the overall structure of warm fronts.

1.1.2.2 Warm Front Models Based on Primitive Equations

Hoskins and West (1979) and Hoskins and Heckley (1981) used semi-geostrophic theory to study frontogenesis. Semi-geostrophic theory combines the geostrophic momentum approximation form of the primitive equations, and a coordinate transformation. The result is a set of primitive equations in which the horizontal advection terms are the geostrophic wind. The ageostrophic flow is obtained by a coordinate transformation back to physical space. Semi-geostrophic theory is described more fully in Hoskins (1975).

Hoskins and West (1979) and Hoskins and Heckley (1981) modelled frontogenesis using a uniform Ertel potential vorticity model with a basic zonal jet flow \bar{u} , where $\bar{u} = 0$ at $Z = 0$ (surface). At $Z = H$ (top of troposphere), \bar{u} varies sinusoidally in space from $1 - \mu$ to 1. Using typical synoptic values, they varied μ and studied frontogenesis as a function of time. They found that for small values of μ (≤ 0.1), a warm front did not develop at all. For $\mu = 0.3$, a weak warm front develops between day 5.5 and day 6 east and southeast of the low center. For larger values of μ , the warm front develops later, and is weaker.

By using an inverted zonal jet flow (i.e. $\bar{u} = 0$ at $Z = H$, and \bar{u} varying sinusoidally at $Z = 0$), a much stronger warm front develops south of the low, associated with the trailing edge of cold air ahead of the low. Further study showed that this warm front had many of the characteristics of a frontal occlusion. Both types of warm fronts (as well as the cold fronts obtained by the model), were very shallow in vertical extent.

1.1.2.3 Previous Observational Studies

In the past, there have been surprisingly few observational studies made of warm fronts. Heymsfield (1979) used the CHILL and NCAR CP-4 radars to study precipitation bands ahead of the surface warm front near Chicago, Illinois. From these observations, Heymsfield found a mesoscale vertical circulation superimposed on the larger scale frontogenetic vertical circulation. This mesoscale vertical circulation was hypothesized to be the cause of the horizontal periodicity in the precipitation bands.

Hobbs and Locatelli (1987) and Hertzman, Hobbs and Locatelli (1988) used doppler radars, rawinsondes, aircraft and surface observations to study a warm front approaching the Washington coast. They found that the warm frontal zone did not lower steadily in height as it approached a coastal location. Instead, there were periods when

the frontal zone was almost level, interspersed with periods when the height decreased sharply. They found that these "steps" in the frontal zone height may increase convergence, and intensify the precipitation bands. The airflow through the warm front was also studied. It was found that, contrary to the traditional view, the warm front was not a boundary through which air could not pass. In fact, airflow through the warm front provided the vorticity to maintain the frontal structure.

2 SYNOPTIC METEOROLOGICAL ANALYSIS

This section describes the synoptic scale meteorological situation prior to, and during the passage of the warm front through Parsons, KS on 25 November 1991. In general, the northeastern two-thirds of the United States was dominated by a strong cyclone located over eastern Canada. A weak intermountain anticyclone was located over the Great Basin (southern Idaho, Utah, Nevada). The cyclone strengthened with height, and the anticyclone weakened with height. These two pressure systems, the eastern Canada cyclone, and the intermountain anticyclone, are normal climatological features associated with the winter season in North America. A stationary front separated these two air masses and evolved into the warm front that was studied.

2.1 Upper Air

The axis of a longwave trough passed through eastern Kansas around 1200 UTC 23 November as shown in the 500 mb analysis (Figure 2.1). The cold air advection associated with this trough dropped the 500 mb temperature at Monett, MO from -13°C at 0000 UTC 22 November to -31°C at 0000 UTC 24 November. By 1200 UTC 23 November, a 500 mb low had formed and was centered near the northeast corner of Kansas. Over the next 36 hours, this 500 mb low moved northeastward to central Ontario, and the 500 mb temperature at Monett, MO rose to -20°C . By 0000 UTC 25 November,

nearly the entire United States was influenced by the geostrophic flow around the longwave trough and its associated low at 500 mb, as shown in Figure 2.2. From 0000 UTC 25 November to 0000 UTC 26 November, significant 500 mb cold air advection occurred over eastern Kansas, with the 500 mb temperature at Monett, MO falling to -26° C. The 310° K isentropic analyses for 25 November at 0000 UTC, 1200 UTC and 1800 UTC are shown in Figure 2.3, Figure 2.4 and Figure 2.5, respectively. These isentropic analyses show increasing heights with time over eastern Kansas, contrary to what would be expected for a warm front. Based on these isobaric and isentropic analyses, we conclude that no warm front occurred on 25 November at 500 mb and above. On 26 November, the 500 mb low moved rapidly northeastward. By 1200 UTC 26 November, the longwave trough no longer dominated the United States, as shown in Figure 2.6. During 26 November, warm air advection occurred over eastern Kansas at 500 mb in advance of a shortwave trough that formed in the east of the Rocky Mountains.

At 700 mb, very weak warm advection was evident at 0000 UTC 25 November, as shown in Figure 2.7. 24 hours later, at 0000 UTC 26 November, pronounced baroclinicity associated with the warm front is noted from eastern Oklahoma to the Canadian border, as shown in Figure 2.8

2.2 Surface

A strong surface cold front passed through eastern Kansas around 2100 UTC 22 November. A surface low formed along the front near Parsons, KS, moved rapidly northeastward along the front, and intensified. By 2100 UTC 23 November, the surface low was near Milwaukee, WI, and moved slowly northeastward thereafter. An arctic high moved southward, and was centered over Saskatchewan at 1200 UTC 24 November. By 2100 UTC 24 November, a well defined stationary front along the lee of the Rockies

separated the arctic air mass from the milder air associated with the intermountain high pressure, as shown in Figure 2.9. There was little movement in the stationary front until around 0600 UTC 25 November, when a weak low pressure trough formed over west Texas. The eastward movement of the intermountain high and the west Texas trough along with the formation of a surface low over Alberta caused the stationary front to evolve into an active warm front by 2100 UTC 25 November, as shown in Figure 2.10. The NWS analysis shows the surface warm front passing through Parsons, KS around 0000 UTC 26 November. The surface warm front moved slowly northeastward, as the surface low over west Texas moved rapidly eastward. By 1800 UTC 26 November, the surface warm front was north of Kansas, as shown in Figure 2.11.

A surface observing station was in continuous operation in Parsons, KS. A time series of the surface temperature for 25 November is shown in Figure 2.12. Observing Figure 2.12, it is not readily apparent when the surface warm front passed through Parsons. The warm frontal passage seems to be obscured by the diurnal temperature cycle. Similarly, the 25 November surface relative humidity shows only the normal diurnal variation. The wind direction time series for 25 November is shown in Figure 2.13. The wind gradually veered from north at 0400 UTC, to east at 1000 UTC, and southeast thereafter. After 1600 UTC, there were wind direction fluctuations between northeast and south. The downward infrared radiation (IR) time series for 25 November is shown in Figure 2.14. Between 0800 UTC and 1500 UTC, the downward IR was nearly constant. As discussed in Section 2.3, this constant downward IR was due to clouds caused by the overrunning of warm air over the cold air. After 1600 UTC, there was a significant decrease in IR as the warm front lowered over Parsons, and overrunning clouds moved north of Parsons.

2.3 Satellite Observations

Hourly infrared satellite images were available for the central United States. At 0300 UTC 25 November, low, broken clouds were observed over northern Oklahoma and southern Kansas, as shown in Figure 2.15. At 0900 UTC 25 November, a broad band of low clouds ran in a northwest-southeast direction from southeast Kansas to southwest South Dakota, as shown in Figure 2.16. This band of clouds was caused by the overrunning of warm air over the cold, arctic air. The southern edge of the cloud band coincides with the location of the surface warm front. Convective activity caused by intensification of the trough is clearly visible over northern New Mexico and Colorado. At 2100 UTC 25 November, the trough has moved eastward into Oklahoma, forcing the warm frontal cloudiness toward the northeastward to northeastern Kansas and Nebraska, as shown in Figure 2.17.

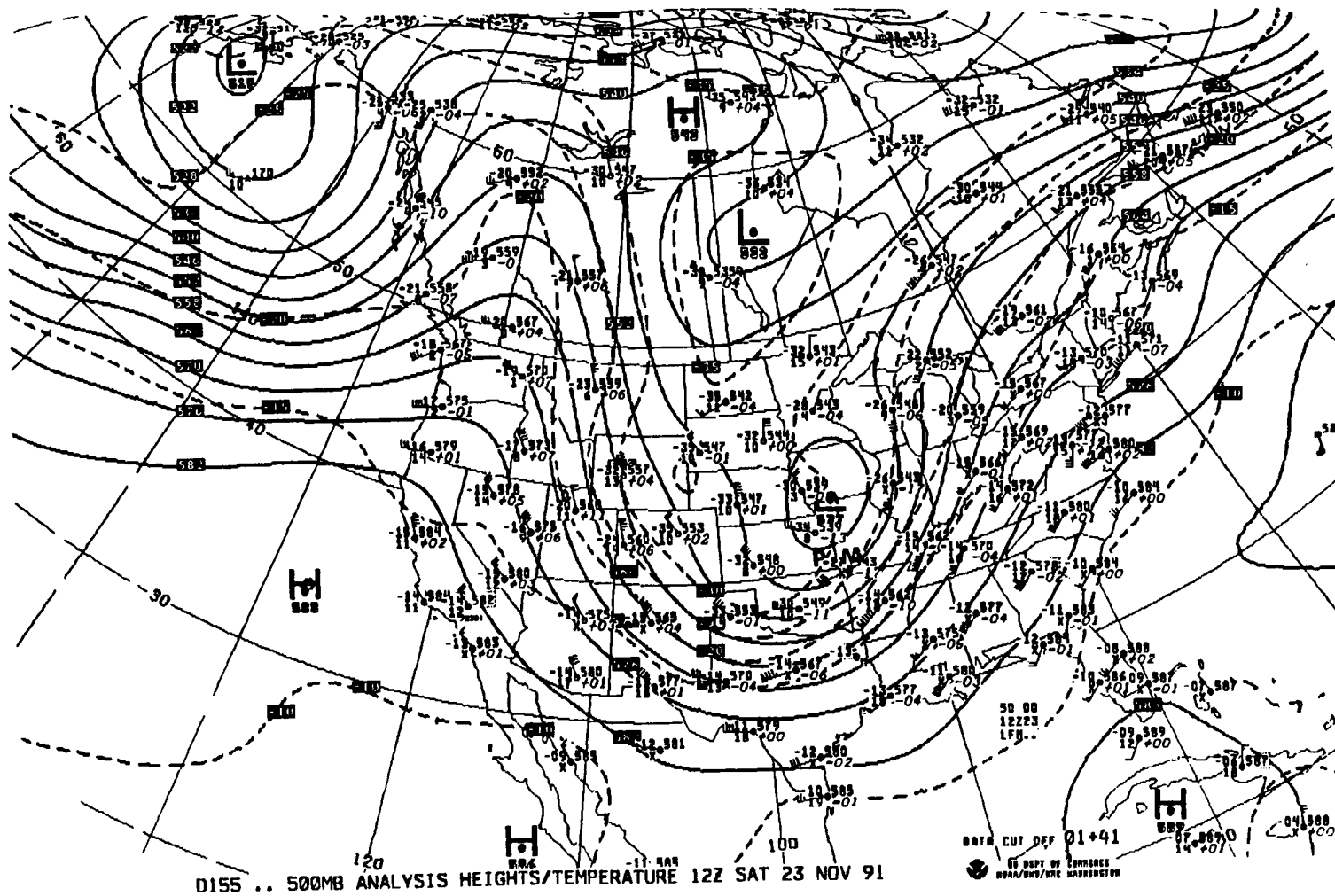


Figure 2.1 - 1200 UTC 23 November 500 mb Analysis. Point labeled "P" is Parsons, KS. Point labeled "M" is Monett, MO.

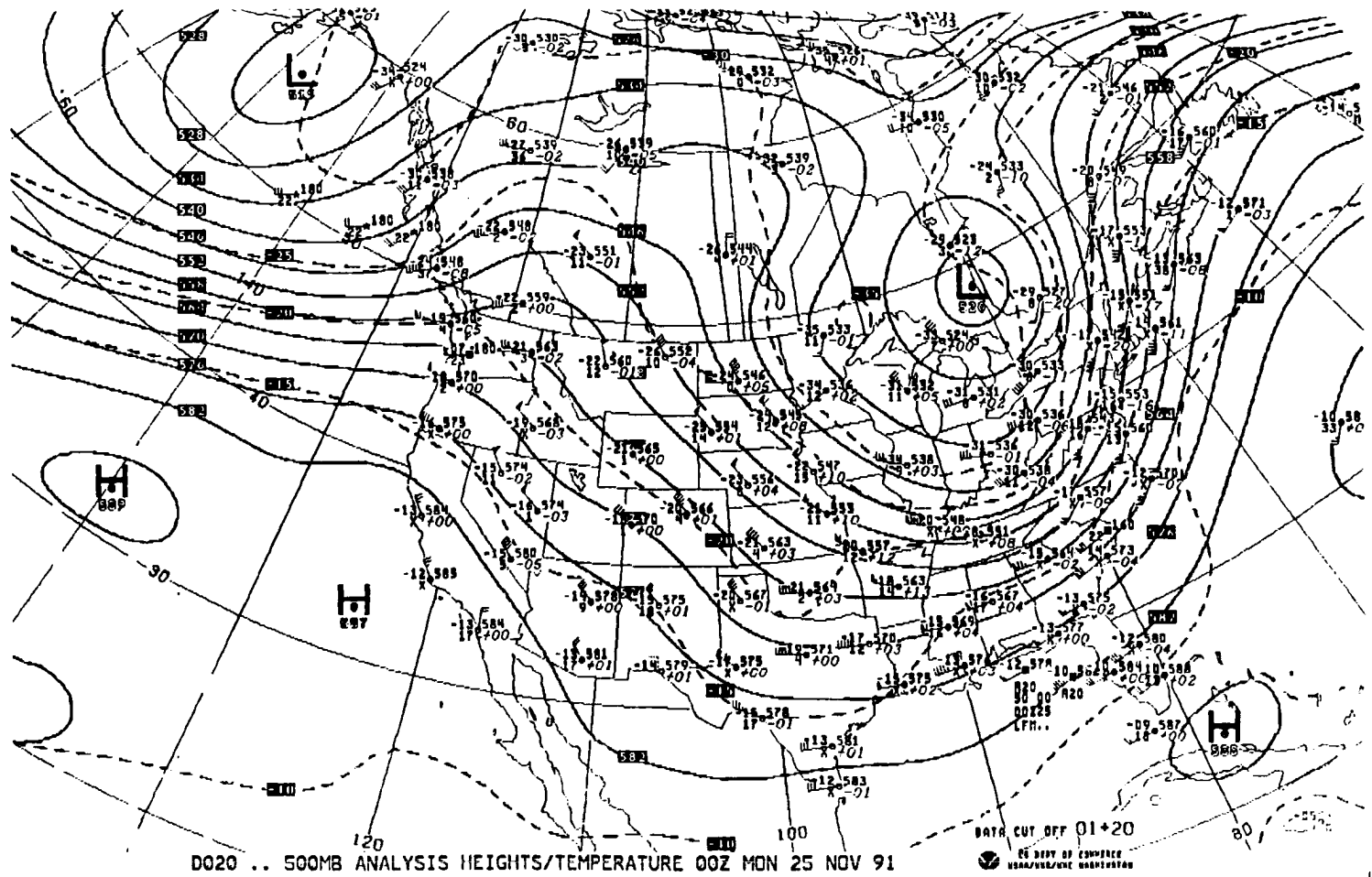


Figure 2.2 - 0000 UTC 25 November 500 mb Analysis

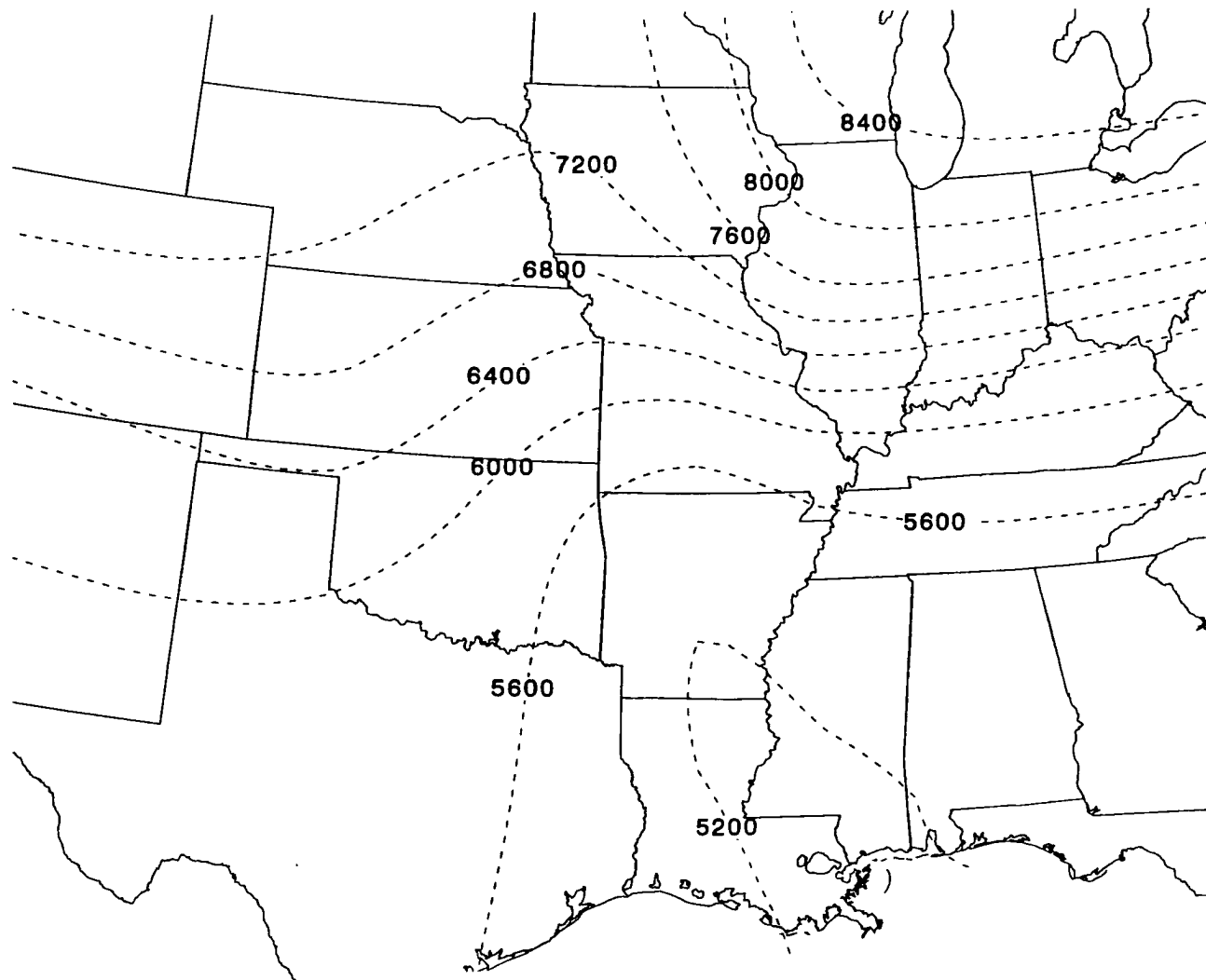


Figure 2.3 - 0000 UTC 25 November 310 Degree Isentropic Height (meters)

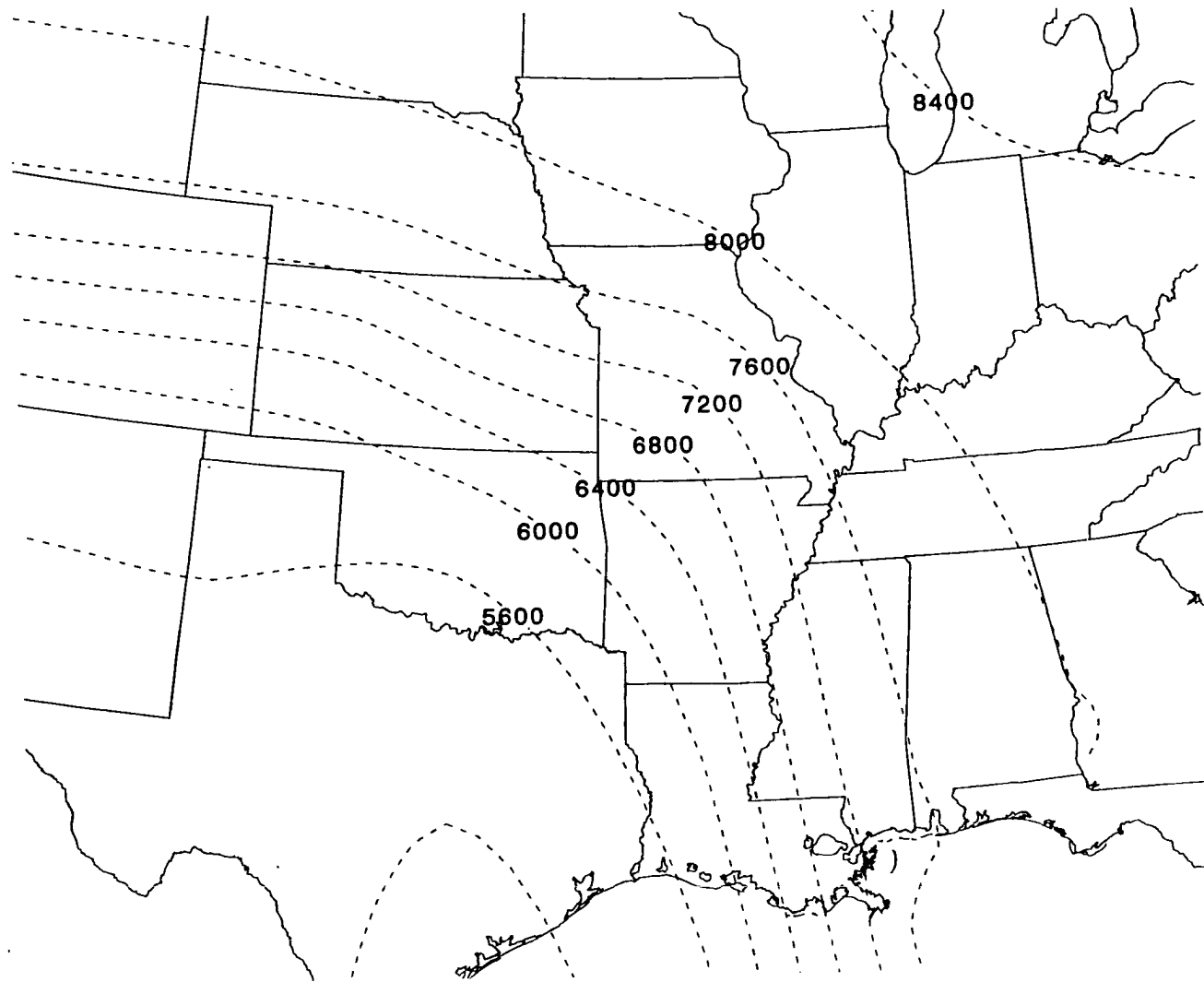


Figure 2.4 - 1200 UTC 25 November 310 Degree Isentropic Height (meters)

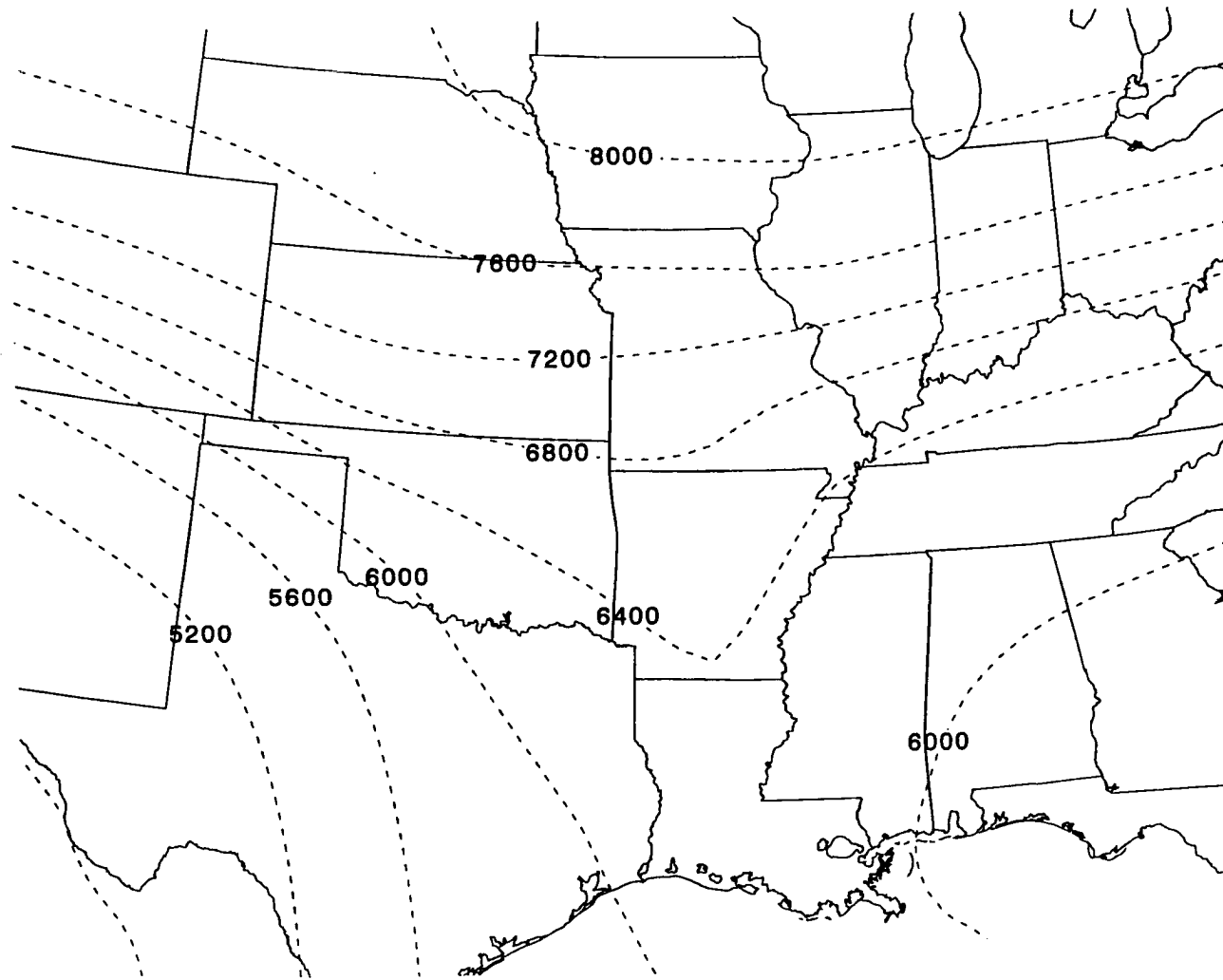


Figure 2.5 - 1800 UTC 25 November 310 Degree Isentropic Height (meters)

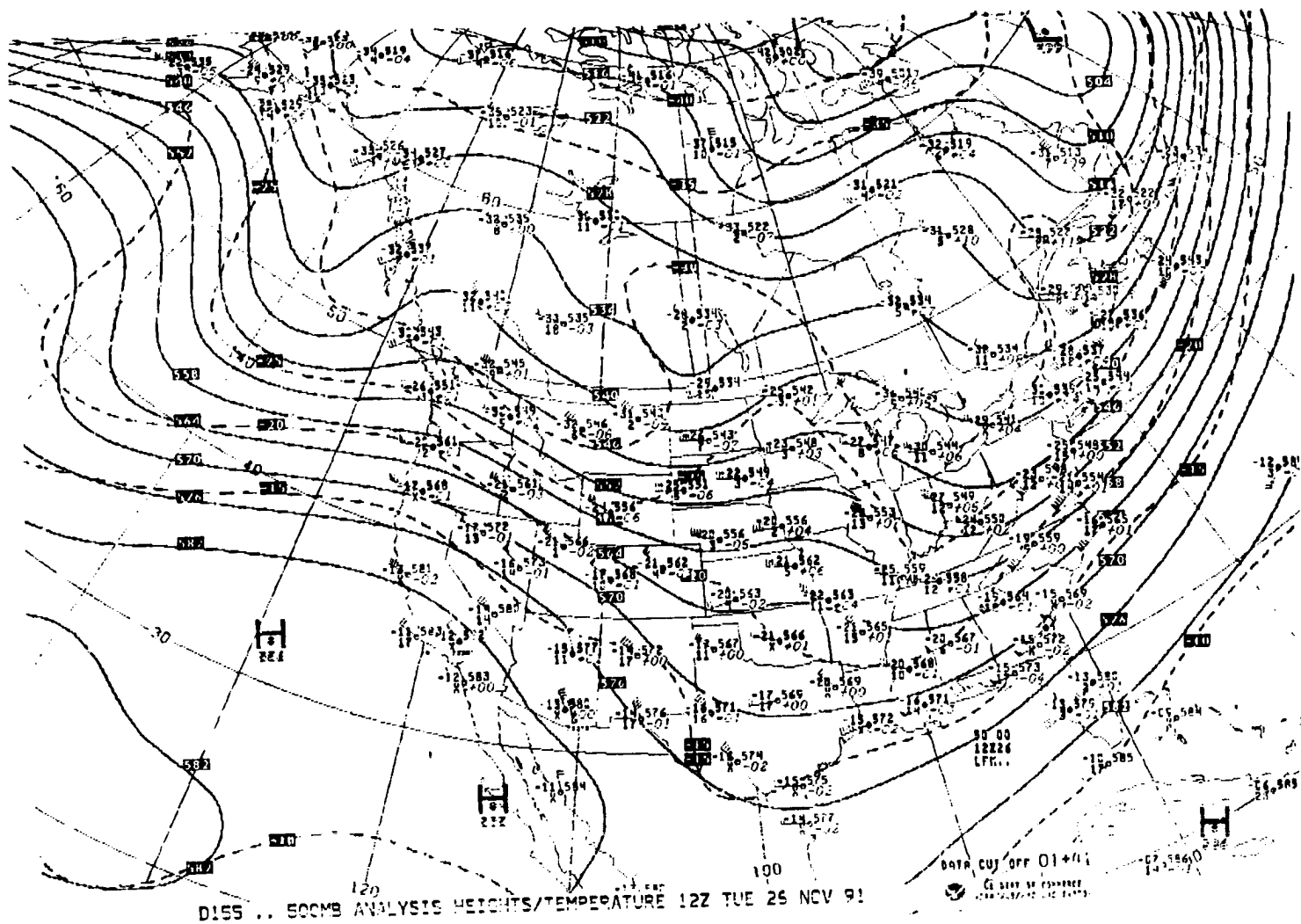


Figure 2.6 - 1200 UTC 26 November 500 mb Analysis

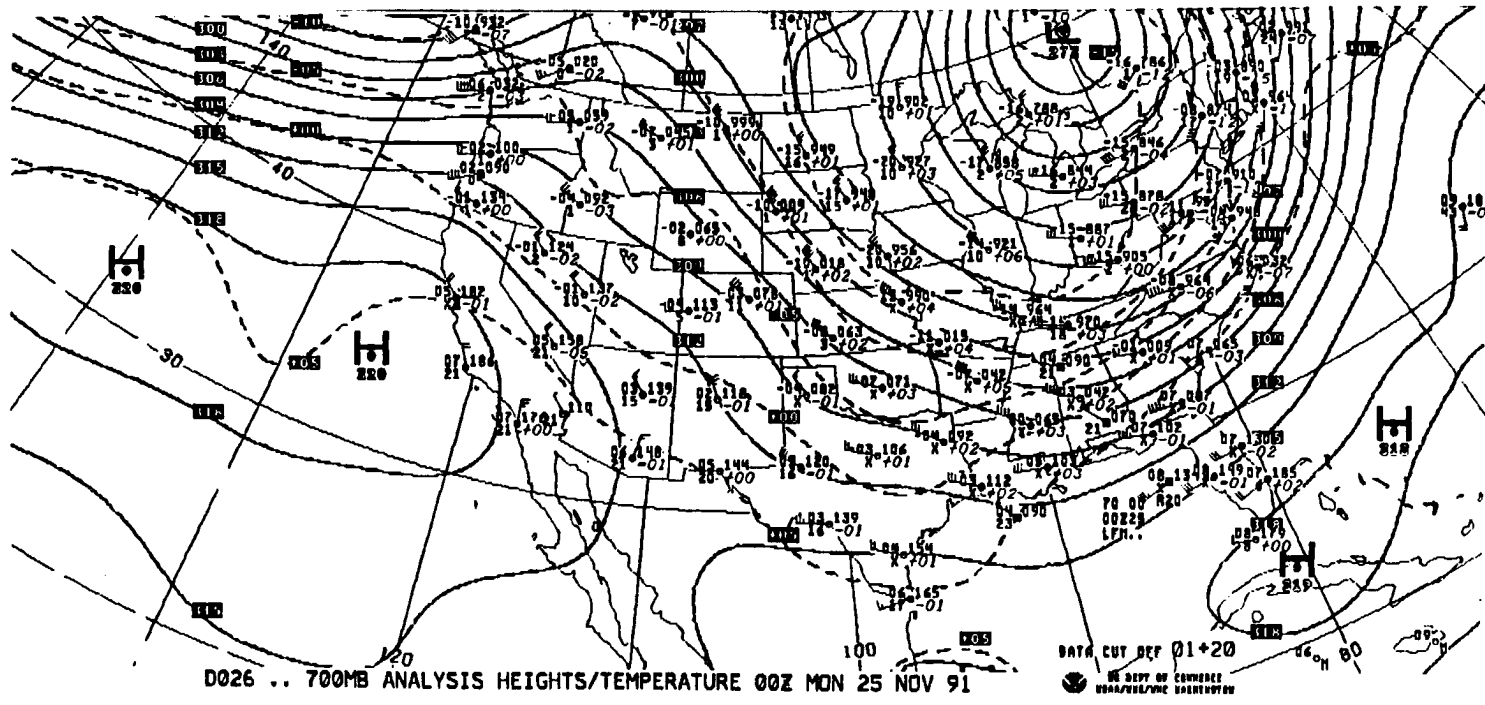


Figure 2.7 - 0000 UTC 25 November 700 mb Analysis

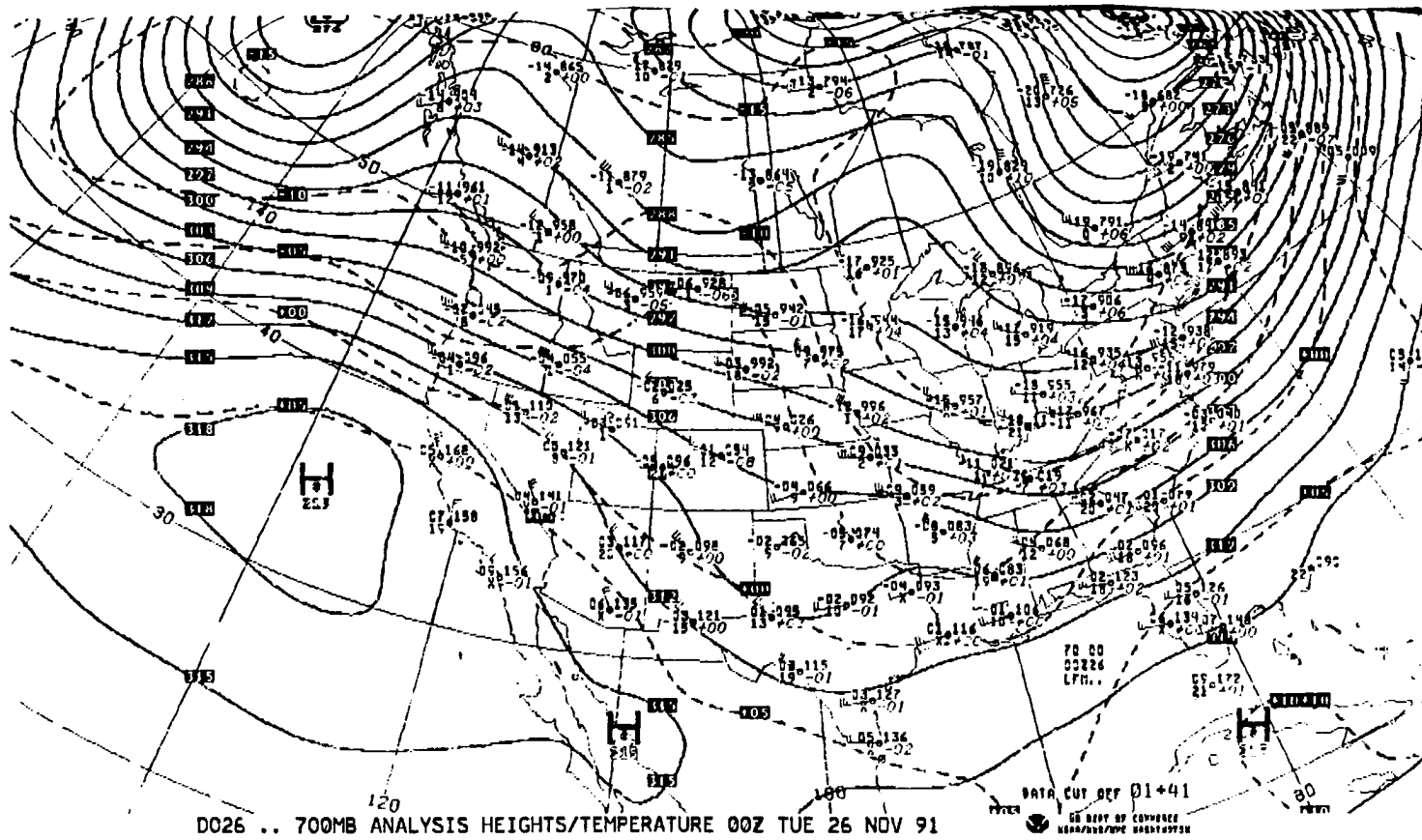


Figure 2.8 - 0000 UTC 26 November 700 mb Analysis

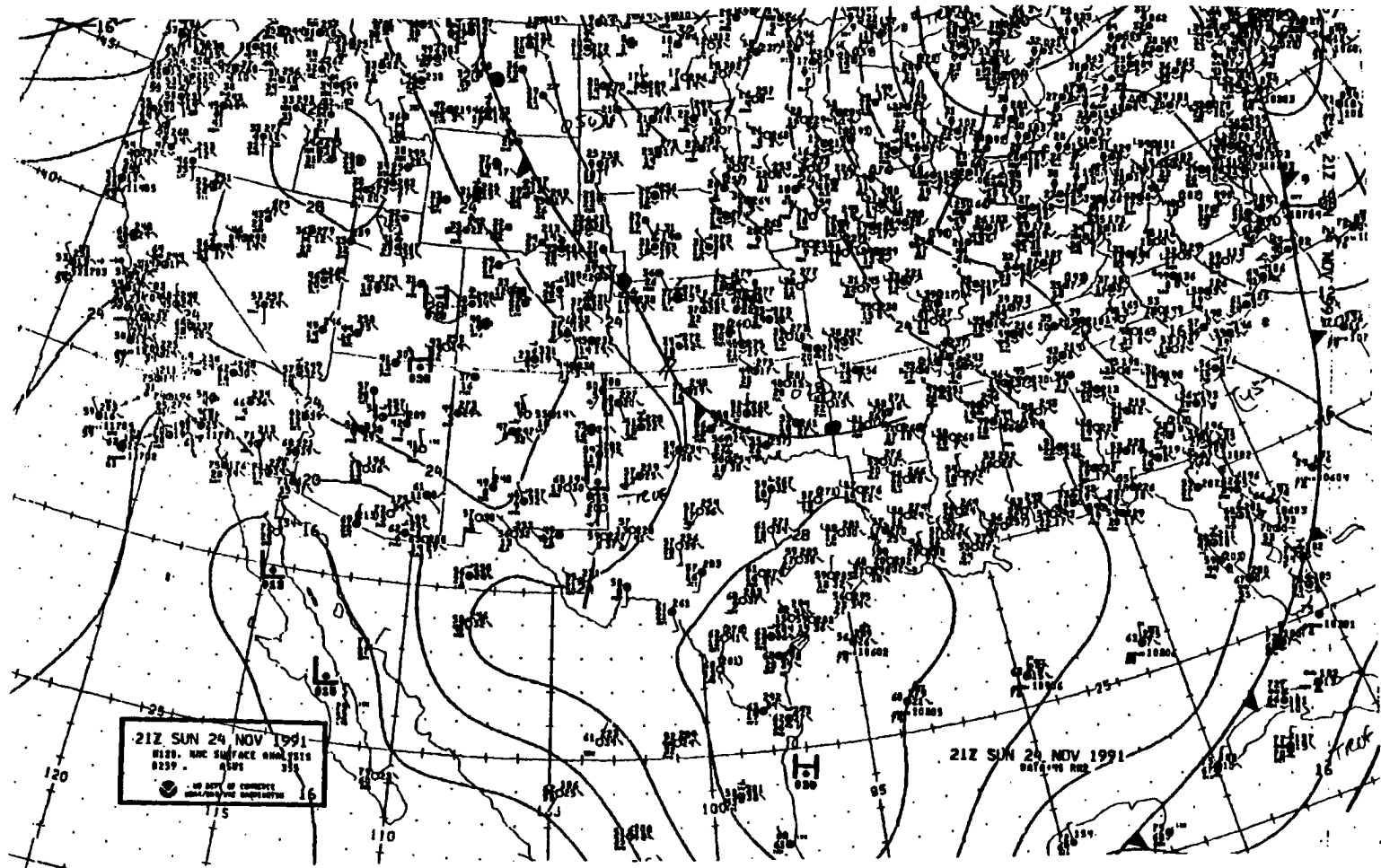


Figure 2.9 - 2100 UTC 24 November Surface Analysis

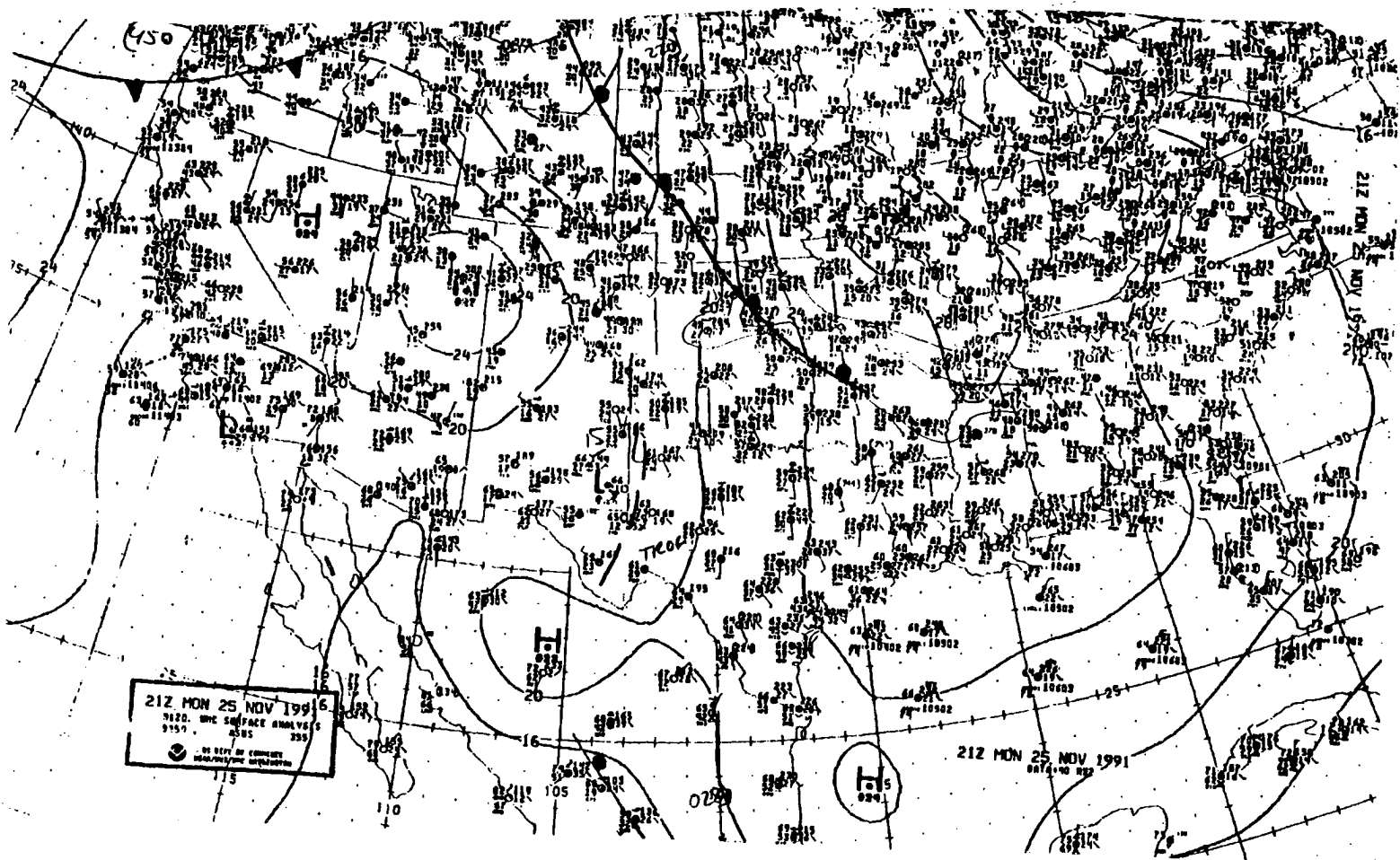


Figure 2.10 - 2100 UTC 25 November Surface Analysis

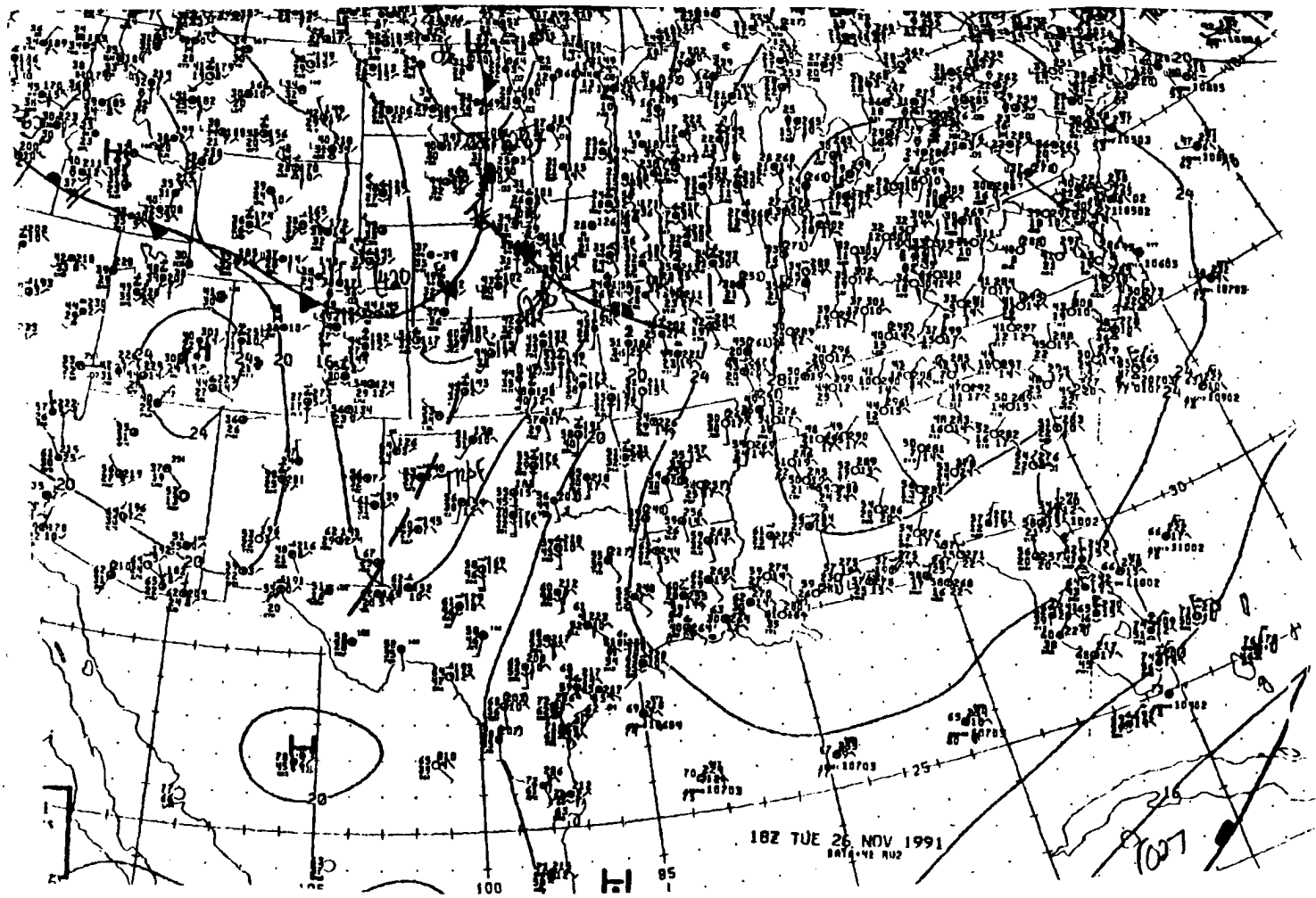


Figure 2.11 - 1800 UTC 26 November Surface Analysis

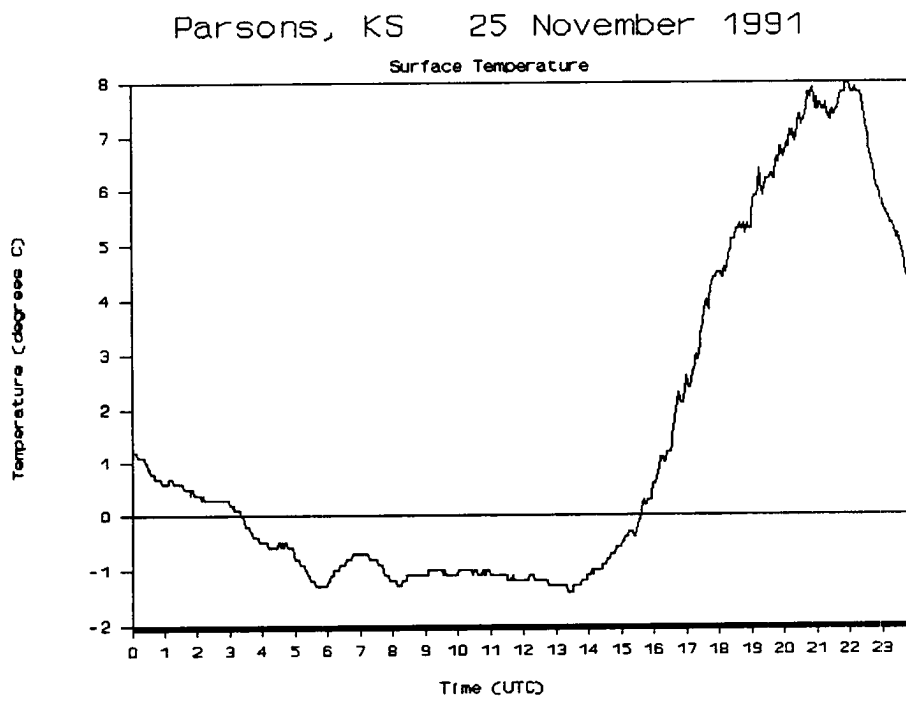


Figure 2.12 - 25 November Parsons KS Surface Temperature

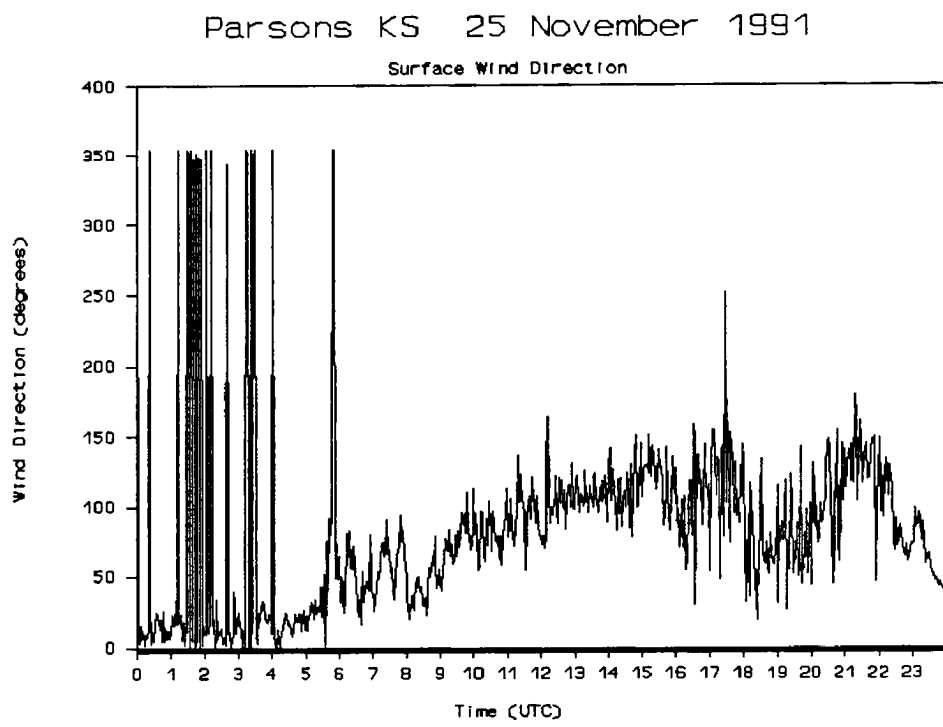


Figure 2.13 - 25 November Parsons KS Wind Direction

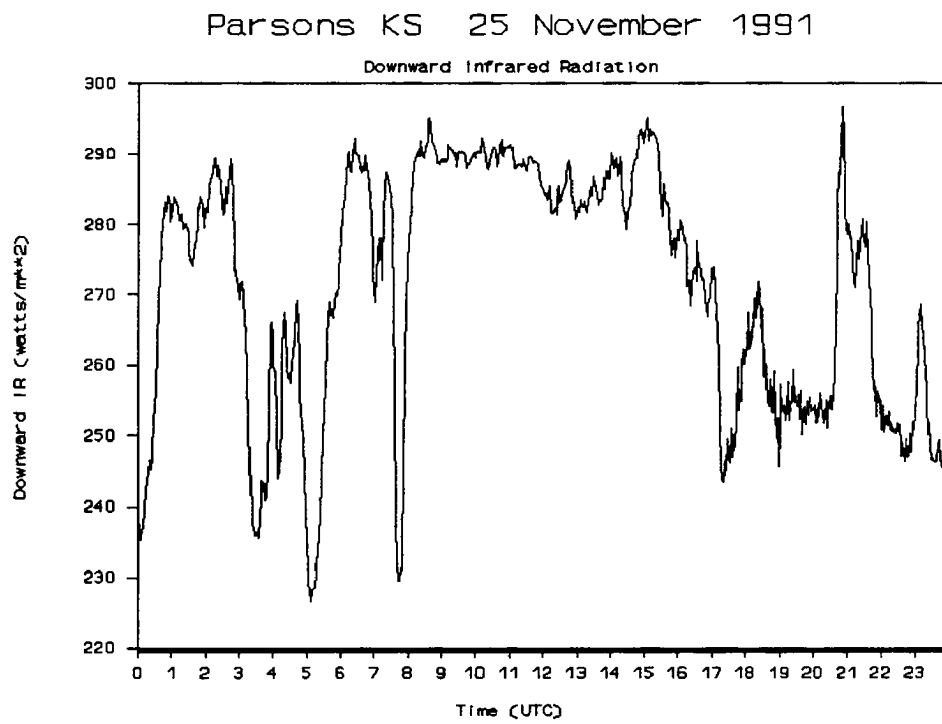


Figure 2.14 - 25 November Parsons KS Downward Infrared Radiation

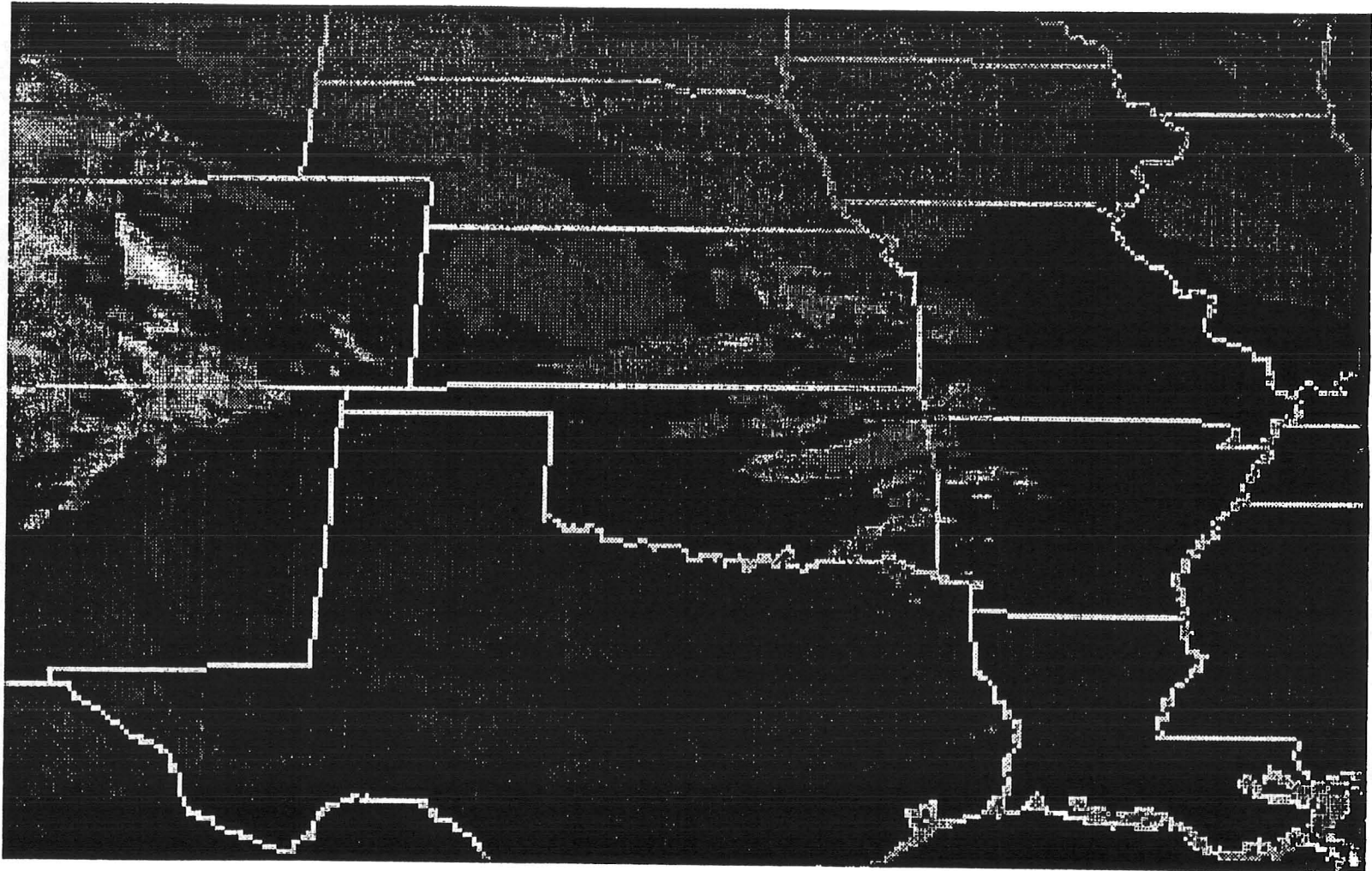


Figure 2.15 - 0300 UTC 25 November Satellite Infrared Image

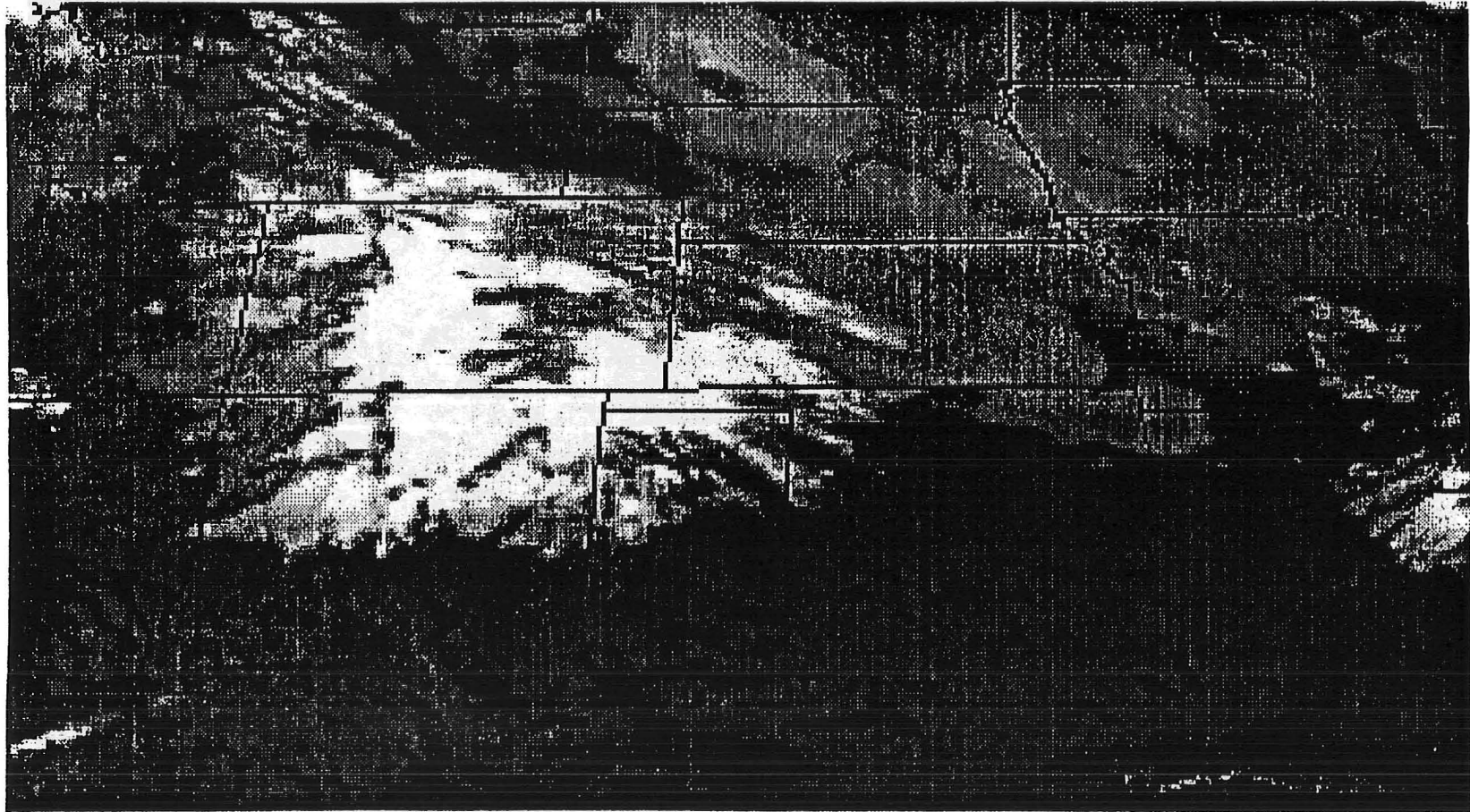


Figure 2.16 - 0900 UTC 25 November Satellite Infrared Image

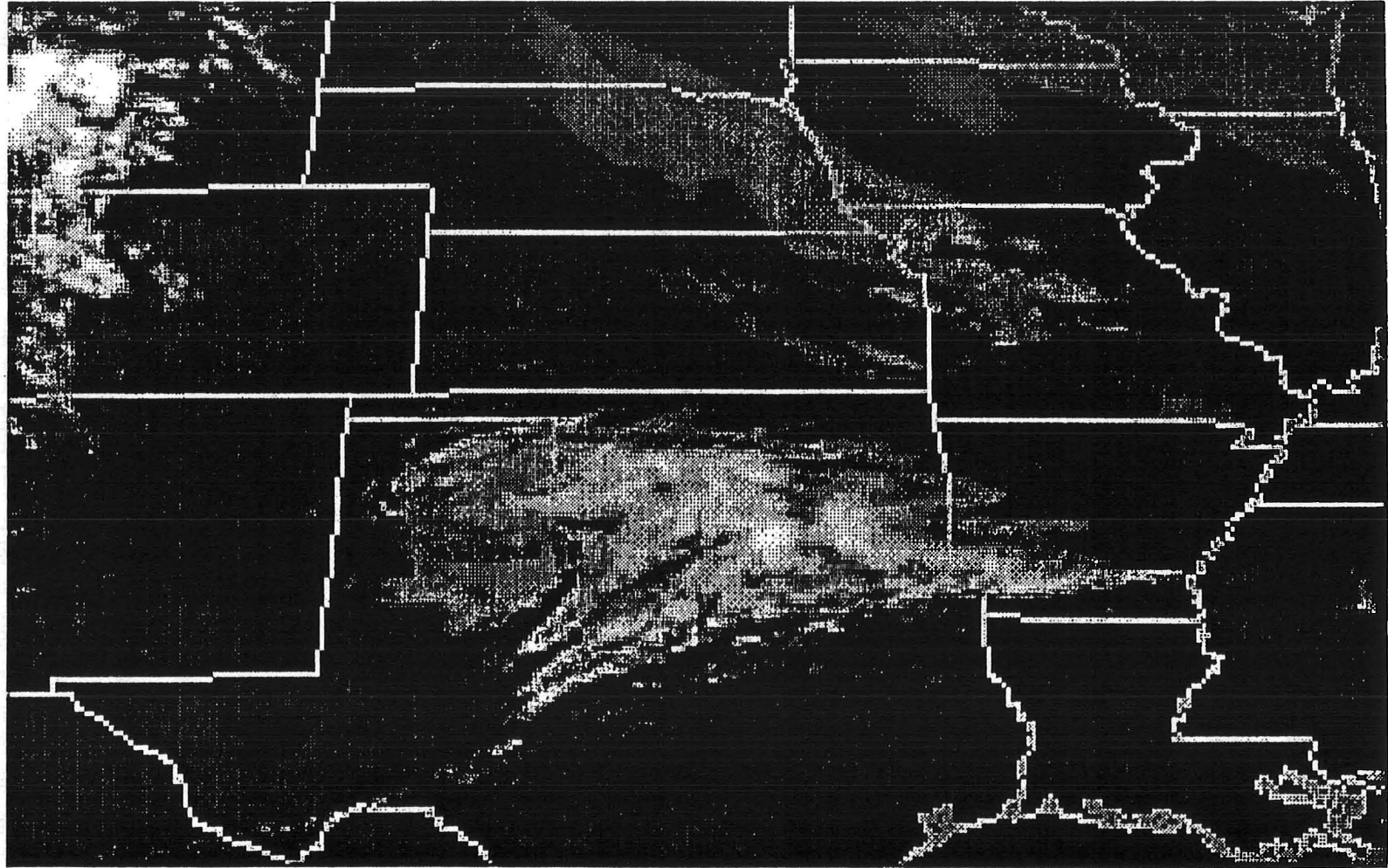


Figure 2.17 - 2100 UTC 25 November Satellite Infrared Image

3 WIND PROFILER OBSERVATIONS, PROCESSING AND ANALYSIS

This section describes the processing and analysis of the 25 November 1991 CSU wind profiler data. The processing of the wind profiler data involved the synthesis of quality-controlled, hourly, wind field averages derived from 6-minute radial velocity and frequency spectrum samples. The analysis of the processed data was used to spatially and temporally locate the warm front.

3.1 Wind Profiler Data Processing

The CSU wind profiler (Tycho Technologies Model 400) was in operation in Parsons, KS from 13 November 1991 until 7 December 1991. The wind profiler output consists of 6-minute averaged spectra and spectral moments for each beam and range gate. The 6-minute averaged spectra contain the signal power in 256 frequency bands around the transmitted frequency, f_o , from $f_o - 128\Delta f$ to $f_o + 128\Delta f$. The 6-minute averaged spectra can be viewed as the raw data from which the spectral moments are derived. Each spectral moment is derived from the averaged doppler-shifted echo returns, and contains the signal power in the peak of the spectra, the average radial velocity derived from the doppler shift at the spectra peak, the variance of the radial velocity around the spectral peak, and the average noise power away from the spectral peak.

The imperfect antenna pattern of any wind profiler, including the CSU wind profiler, results in many sidelobes that transmit pulses and receive echos. In particular, there are sidelobes present at very low horizon angles that receive strong echos from stationary, or near-stationary objects near the ground. The resulting frequency spectra has a very strong peak near the transmitted frequency, f_o . Any attempt to extract the spectral moments from the spectra must first filter out the "ground clutter" that caused this "central

peak". Filtering out the signal power in frequency bands near the central peak can result in the loss of information on very low wind speeds.

To derive the vertical wind speed in the high-resolution, low height mode, the unfiltered 6-minute frequency spectra was used. The spectral moments were derived, with only the ground clutter filtered out. The derived vertical radial velocity moments were found to either be less than 1 m/s, or very large (typically greater than 10 m/s). The large velocities always had large variances, and low signal-to-noise ratios. These large values were probably indicative of very low vertical velocities that were perceived as ground clutter by the wind profiler filtering algorithm. Therefore, any derived vertical velocity of greater than 1.2 m/s was set to 0 m/s. The derived vertical wind speeds were averaged over three adjacent height levels.

For the low-resolution, high height mode, an inspection of the unfiltered 6-minute frequency spectra typically did not show a discernable power peak. Therefore, the high mode vertical velocities were assumed to be zero. The error introduced by this assumption should be negligible, since the non-vertical beam radial velocities in the high mode were large.

The derived vertical beam spectral moments were merged with the non-vertical beam spectral moments to create a composite spectral moment data set.

The quality control algorithms described in Section 1.1.1.1 were studied in relation to the composite spectral moment data set. The following quality control algorithms were applied to the 6-minute spectral moment data sets:

- All data during the 6-minute cycles that RASS sound waves were generated were marked as bad.

- Shear checking was used to remove wind vectors that differed significantly from their spatial and temporal neighbors.
- Radial velocity variance was checked. Radial velocity variance moments that did not exceed a minimum variance were removed.
- Horizontal homogeneity of the wind field was tested by deriving four wind velocities from the 5 beams. If the four derived wind velocities varied significantly, all radial velocities for that time and height were marked as bad.

Hourly averaged radial velocities were obtained from the post-quality control 6-minute radial velocity moments using the following procedure:

- For hours in which there were two or more 6-minute spectral moment data sets, the radial velocity spectral moments at each height level were averaged, provided there were two or more valid radial velocity spectral moments at that height. When there was only a single valid spectral moment at a height level, that height level was not included in the hourly average.
- For hours in which there was only a single set of 6-minute spectral moments (1800 UTC and 1900 UTC), this single 6-minute spectral moment became the hourly average.

The following quality control algorithms, used by other researchers, were *not* applied to the Parsons wind profiler data:

- Consensus averaging was not used to obtain hourly averages. For the 25 November time period, each hour contained from one to six 6-minute spectral moment data sets, rather than the 10 data sets per hour available from the NOAA profiler demonstration network. For hours when there are very few data sets available, the credibility of the consensus averaging technique is questionable.
- The continuity technique is a more mathematically rigorous method of shear checking. The additional complexity of the continuity technique did not seem warranted vs. the Hein (1991) shear checking technique that was applied.

3.2 Warm Front Placement Using Wind Profiler Data

The quality controlled, hourly averaged, radial velocity data from the Parsons wind profiler for 25 November were used to plot the time series of wind velocity shown in Figure 3.1, Figure 3.2, and Figure 3.3.

Warm advection, as indicated by veering winds, is first notable at 0600 UTC near 3 km (point "a" in Figure 3.1). The base of the layer of veering winds remains at the same height, but widens from 0700 UTC until 1000 UTC (point "b" in Figure 3.2). From 1100 UTC until 1400 UTC, the veering wind layer continues to broaden and lower. After 1500 UTC, the base of the veering wind layer is below the lowest profiler range gate. Based on the convention of Hobbs, et al. (1987), the warm frontal zone is defined as the layer of veering winds, with the warm front located at the top of the warm frontal zone. The 25 November warm front appears to be confined to the lower troposphere. This is made particularly apparent by the study of the temperature advection profile in Section 3.3.